NeuroMaps – A Compact Fingerprint for Analyzing Brain Activity

S. Lengauer[1], B. Kantz[1], P. Waldert[1], G. Tussardi[1,2], N. Kohn[3], and T. Schreck[1]

[1]Graz University of Technology, Institute of Visual Computing, Graz, Austria
[2]University of Padova, Department of Information Engineering, Padova, Italy
[3]Radboud University Medical Center, Donders Institute for Brain, Cognition and Behaviour, Nijmegen, Netherlands

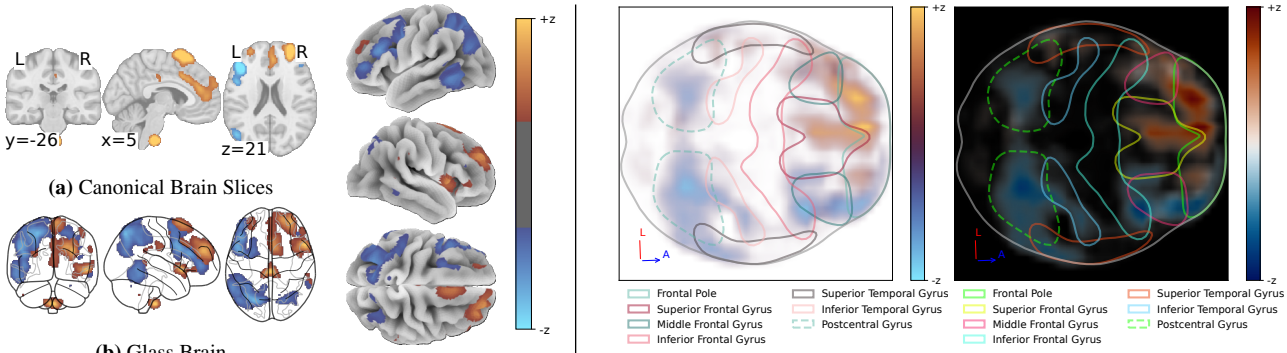

(a) Canonical Brain Slices **(b)** Glass Brain **(c)** Surface Rendering **(d) NeuroMaps**

Figure 1: Common techniques for visualizing differences in brain activities, such as (a) canonical slices, (b) glass brains, or (c) surface renderings require multiple views or sectional cuts for a comprehensive overview on the overall activity patterns. In contrast, our proposed NeuroMaps (d) consolidate this information into a single, dense saliency visualization enhanced by parcellation outlines and additional visual cues for providing context. We propose distinct light and dark color schemes, optimized for print and on-screen display, respectively.

Abstract

Readings of differences in statistical brain activity obtained from task-based or task-free neuroimaging experiments provide essential insights for a wide range of neuroscientific analyses, including the study of cognitive functions and the comparison of activity patterns across cohorts of individuals. Over the past decades, visualization techniques to show activity within the three-dimensional brain volume have been developed. Most approaches have in common that they rely on multiple views to imply spatiality, asking users have to mentally integrate them in order to achieve a coherent holistic understanding. This process is particularly demanding if the results of several experiments are examined in conjunction for comparative analyses. We propose NeuroMaps – a compact fingerprint design which summarizes spatial activity patterns in an intuitive and space-efficient manner. By integrating all relevant information in a single image, NeuroMaps enables neuroscientists and other experts to quickly obtain a coarse overview, rendering it a particularly useful tool for comparing large sets of neuroimaging results.

CCS Concepts

• ***Applied computing*** → ***Bioinformatics;*** • ***Human-centered computing*** → ***Scientific visualization;***

1. Introduction

Brain functional imaging relies on different capturing techniques such as functional Magnetic Resonance Imaging or Electroencephalography to obtain estimates of brain activity in both spatial and temporal dimensions. For the process of examining differences in these activities – known as Statistical Parametric Mapping (SPM) – different neuroimaging methods have been developed which plot voxel-wise, parcellated or otherwise grouped statistical values derived from task-based or task free experiments onto the brain's topological structure. This is used by neuroscientists and other experts to pinpoint relevant areas, study cognitive functions, or investigate (dis)similarities across cohorts of individuals. Traditional solutions to this end, are canonical slices through the so-called *gray-matter brain*, overlayed with a color coding for statistical values (Fig. 1a), (semi)transparent or solid 3D renderings

(Fig 1b and 1c), projections of the cortical layer, projections in embedding space, or combinations thereof. They suffer from the downside that multiple sources of information (i.e., multiple images) need to be considered simultaneously and mentally integrated in order to obtain a holistic understanding of spatial activity patterns. Such requires continuous content switching, inducing a significant cognitive load [CS92]. In many analytical use cases such as between-subject comparison, this problem is aggravated, as not a single brain activity is considered, but several simultaneously.

Glyphs and *visual fingerprints* are an effective approach to convey complex properties of data units in a compact manner [CS25]. We follow this direction by introducing *NeuroMaps* – a novel compact fingerprint, showing the 3D image of statistical brain activities integrated along a projection axis which maximizes between-region separation as a planar map of saliencies (Fig. 1d). Additional visual cues such as contour outlines of coherent structural or functional regions, the outline of the whole brain, and a compass relating the projection to the dimensions of the 3D brain, allows users to perceive the brain morphology. Even though this does not allow for a precise analysis in complex cases, it can serve as an intuitive compact preview when reviewing numerous different results.

2. Related Work

The most basic (non-visual) technique of SPM is to use tabular representations of coordinates of the most significant differences [Smi04]. Due to the limited scalability and analysis capabilities of this kind of representation, graphical variants quickly emerged with colored activity 'patches' overlayed on a gray matter brain image [FHW*94] (Fig. 1a) being among the first visual solutions. Slices through the 3D volume are commonly placed at representative locations, corresponding to *sagittal*, *coronal*, and *traverse* cuts. The coloring of patches is used to reflect statistical values, such as t-values or z-scores. A limitation is that solely activity in the vicinity of the cut planes is visible. The so called *Glass Brains* [Mad15] or Maximum Intensity Projection images (Fig. 1b) propose a solution to this problem, by integrating over the activities along the view axis (perpendicular to the cut plane). In the example, it can be observed that this method is able to reveal several hidden activity clusters, but still faces challenges if both positive and negative values are aggregated. The projection step of the NeuroMaps is inspired by this idea, but – opposed to having fixed projection axes – we determine an *activity-based projection*, leading to a maximal separation between clusters of common activity and region.

Other common visualizations are surface-based, i.e., 3D renderings of the gray-matter brain (Fig. 1c), with respective heatmaps for indicating active regions. There are also dedicated solutions for the cerebral cortex, the outermost wrinkled area of the brain responsible for many high-level functionalities. Due to its thin layered morphology it is often treated as a surface and thus visualized as a 'flattened' or 'unfolded' 2D image known as *cortical sheet* or *cortical flat map* [DVEA*96]. Bolaños-Puchet et al. [BTH*24] combine this unfolding idea with a projection scheme to generate intuitive laminar brain atlases for the isocortex of the mouse. For specific fields of neuroscience, such as neuropharmacology, human genetics, or neuroanatomy, a gene expression map, such as the Allen Brain Atlas [HLG*12] are used.

Several open-source software solutions, such as the *Multi-image Analysis GUI* [HLM], support the generation of above-mentioned visualizations. Both *MRIcron* [Ror25] and *nilearn* [CFR*26] provide encompassing tool sets for creating slices, mosaics, surface renderings and glass brains. The browser-based *neurovault* [GVR*15] allows the interactive analysis and sharing of arbitrary brain images, while the (also browser-based) *neuroglancer* [MBS*21] also implements complex visualizations such as for the brain's connectome [SYB*24].

3. The NeuroMaps Design

The pipeline for generating the NeuroMaps consists of three core steps, as shown in Fig. 2: (i) an (optional) morph step (Sec. 3.1), slightly altering the 3D brain structure into a more favorable shape leading to a better separation of structural brain regions; (ii) a projection step (Sec. 3.2) for finding an optimal projection angle; and (iii) a postprocessing step (Sec. 3.3) for computing saliencies in projection space and drawing additional visual anchors. As input we require both brain activity based on a stimulus and a parcellation – labels organizing the brain into functional or structural units. Regarding the prior, a Voxel-wise Encoding Model (VEM) [DLTV-DOCG25] can be used to translate a signal obtained from a certain stimulus into voxel-wise brain activity. This is, however, beyond the scope of this paper, as we assume to receive this input in already-translated format, which is the common output of respective studies. The established standard to this end (MNI-152 [FEB*11]) defines an isotropic voxel grid $\mathbb{R}^{N_x \times N_y \times N_z}$ with $N_x = 91$, $N_y = 109$, $N_z = 91$ or $N_x = 182$, $N_y = 218$, $N_z = 182$, corresponding to physical voxel resolutions of 2 mm or 1 mm, respectively. The same file format is common for parcellations.

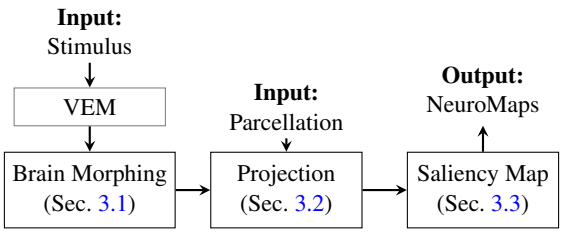

Figure 2: Schematic overview of the processing pipeline.

3.1. Brain Morphing

This step is optional, but we observe that in cases where many regions exhibit activity, even the optimal projection sometimes results in several overlapping regions. Spherical projection has been used to untangle the regions close to the cortical sheet [AWW*23]. This morphing is, however, not beneficial for the whole brain. Instead, we investigate a different modification for maximizing the separation between structural components. As the morphology of the human brain can be approximated by a dome, we employ a combined 'explosion' movement, corresponding to a azimuthal equidistant projection [SV89] in the horizontal plane, and vertical movement in dorsal direction.

Let $V = v \subset \mathbb{R}^3$ be the set of voxel locations in 3D space.

$\tilde{v} = \begin{pmatrix} \varphi \sin\lambda & -\varphi\cos\lambda & \alpha v_z \end{pmatrix}$ is v's corresponding morphed position, with φ as v's 'azimuthal' angle w.r.t. the volume's center $C = \begin{pmatrix} N_x/2 & N_y/2 & N_z/2 \end{pmatrix}$ in the horizontal plane and λ as the 'elevation' angle spanning between $v - C$ and the superior direction. α governs the strength of the vertical movement and $\theta(v) = \exp\{-\frac{\|v_{xy} - C_{xy}\|}{2\sigma_z^2}\}$ is a fast-decaying drop-off kernel for governing the influence of the offset from the center, ensuring that regions far away from the 'core' of the brain are only mildly affected.

This kind of morphing results in a completely deformed brain topology, we empirically discovered, however, that slight transformations based on a linear interpolation between v and $\tilde{v}$ yield a good tradeoff between fidelity and clarity. That is, we define the interpolated mapping $\pi^\beta(v) = v + \beta(\tilde{v} - v)$ governed by β, with $\pi^0(v) = v$ and $\pi^1(v) = \tilde{v}$ (Fig. 3).

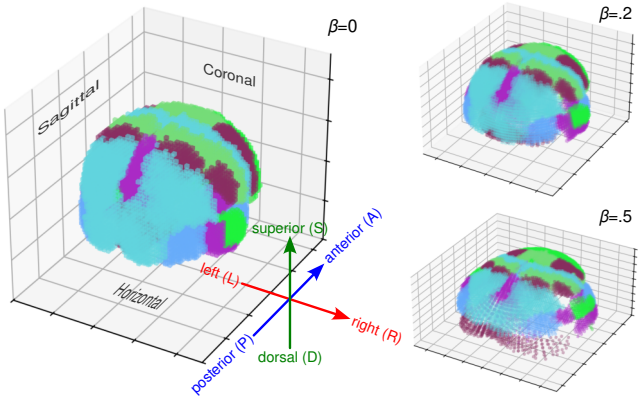

Figure 3: For morphing the brain a vertical movement in dorsal direction is combined with an explosion movement reminiscent of a azimuthal equidistant projection in the horizontal plane. Left: brain volume in its original state with the different colors for parcellation regions. Right: The brain topology at different stages of morphing.

3.2. Projection

To determine a projection axis, which maximizes separation between regional activity clusters, we leverage Fisher's Linear Discriminant Analysis [Fuk13], which was generalized by Rao [Rao48] to support multiple classes. This linear dimensionality reduction algorithm defines a criterion

$$J = \frac{\omega \Sigma_B \omega^T}{\omega \Sigma_W \omega^T}, \tag{1}$$

maximizing the ratio between the between-class covariance Σ_B and the within-class covariance Σ_W. We obtain the class-separation vector ω, which is used as the projection axis, through the eigenvector decomposition of $\Sigma_W^{-1}\Sigma_B$. The between-class covariance is given by

$$\Sigma_B = \sum_{n=1}^{|K|-1} \sum_{m=n+1}^{|K|} p_n p_m (\mu_n - \mu_m)(\mu_n - \mu_m)^T, \tag{2}$$

with K as the index set of classes, and μ_n, μ_m and p_n, p_m as the mean vectors and priori probabilities of classes n and m, respectively. Conversely, the within-class covariance is defined as

$$\Sigma_W = \sum_{k=1}^{|K|} \sum_{i \in C_k} (\pi^\beta(v_i) - \mu_k)(\pi^\beta(v_i) - \mu_k)^T. \tag{3}$$

To narrow down the analysis to brain regions experiencing the most stimulus, it is common to subject the activities to a threshold. As the considered activities $\mathcal{A} \subset \mathbb{R}^{N_x \times N_y \times N_z}$ are typically signed, we subject both the mask of voxels exceeding a given threshold (i.e., positive mask) and the mask of voxels below the threshold (i.e., negative mask) to a 26-connected neighborhood 3D connected components analysis [Sil21] and unify the resulting index sets. 6 and 18-connected neighborhood were also tested, but lead to a higher fragmentation and overall inferior results. With K as the index set of components, we define $\{C_k\}_{k \in K}$ as the set of mask indices for all component K. We can thus define the mean vector and priori probability for k as

$$\mu_k = |C_k|^{-1} \sum_{i \in C_k} \pi^\beta(v_i) \quad \text{and} \quad p_k = \frac{\sum_{i \in C_k} |\mathcal{A}_i|}{\sum_{k'=1}^{K} \sum_{i \in C_{k'}} |\mathcal{A}_i|}, \tag{4}$$

respectively. Solving Eqn. (1) for ω gives the corresponding projected positions $Y = \omega\{\pi^\beta(v) \in V\} \subset \mathbb{R}^2$.

3.3. Saliency Map

To visualize the activities in projection space, we use a saliency map which is generated by integrating $\mathcal{A}$ along the projection axis ω. After binning Y, a bi-directional histogram is computed over the integrated activities. As the t-values and z-scores exhibit both positive and negative intensity peaks, separate histograms are computed over $|\mathcal{A}|$ and $\mathcal{A}$ to differentiate between bins with overall high activity from bins where positive and negative contributions cancel each others out. While the prior are encoded in NeuroMap's alpha channel (rendering regions without activity transparent), the latter serve as input for a perceptional uniform diverging color scheme [Cra18], allowing to distinguish between regions of positive, negative, or mixed activity.

A NeuroMap comprises additional visual cues which allows neuroscientists to put the displayed activities into context (Fig. 1d). That is, a contour outline of the whole brain is drawn alongside contours of functionally or structurally distinct regions, having a substantial overlap (based on a given threshold) with the activities. Said regions are given by brain parcellations, which organize brain volumes in labeled regions. To date, many different parcellations, obtained though different methods, are available [AKM*18]. In all shown examples, one carefully selected parcellation (https://neurovault.org/images/1699/) from the *Harvard-Oxford cortical and subcortical structural atlases* collection [DSF*06, FCB*05, GSM*07, MGK*06] was used (Fig. 3). The approach, however, is independent from the choice of parcellation. The contour outlines of the affected regions are detected in projection space after subjecting the affected regions to the same projection as the activity. The external contours of the rasterized region masks are detected [Sb85], filtered, and subjected to a smoothing [SG64] to remove high-frequency jitter. For connecting outlines to a legend, we use a qualitative color scheme generated by *Colorgorical* [GLS17] after filtering out hue ranges already used

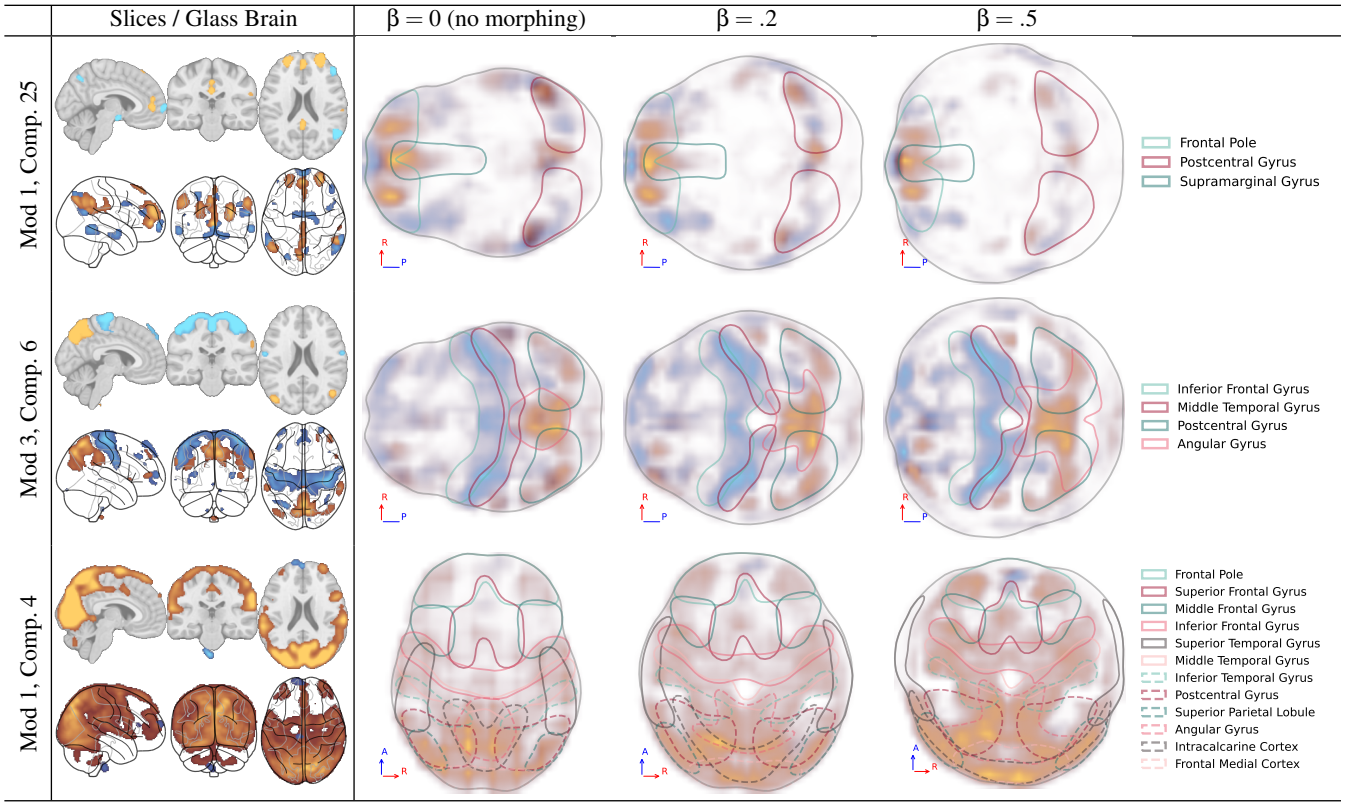

Figure 4: Three selected z-scores results from a linked independent component analysis showing vastly different activity patterns. In each row we show the 'baseline' references of canonical brain slices and glass brains alongside the NeuroMaps without morphing and with $\beta \in \{.2, .5\}$. The color coding of the saliencies follows the colorbars given in Fig. 1 for slices, glass brains and NeuroMaps, respectively. Additional examples are provided in the supplementary material.

by the underlying saliency map. As qualitative schemes reach the limit of minimal discernible difference with up to 6 different colors [WQZ*25], we use the line style of contour as secondary channel if more regions are of relevance. To convey a sense of depth, the contours are drawn in reverse order to their region's offset along ω. Lastly, a compass indicating the projection plane w.r.t. the canonical brain axes (c.f., Fig. 3, left) is drawn in the bottom left corner of the fingerprint.

4. Use Case Example, Limitations, and Future Work

For showing the effectiveness of the NeuroMaps design, we present three carefully selected examples (Fig. 4) of z-scores from a linked independent component analysis of gut microbiota and brain activity [KSLA*21], exhibiting different inherent challenges. The code for generating the NeuroMaps is available at `https://github.com/lenxn/neuromaps.git` under the MIT license.

We observe that in most cases the projection strongly aligns with the sagittal, coronal, or horizontal plane, which we attribute to the mirror-symmetrical nature of most activities. The NeuroMaps appear particularly useful in cases where activity is focused in a few selected linearly separable regions. In cases of severe region-overlap in the projection space (e.g., Fig. 4, bottom row), the differentiation between regional activity clusters is impaired. Brain morphing can solve this problem to some extent, but requires further investigation. Driven by an objective function such as overall region overlap, our next step will focus on the development and analysis of more refined methods to this end.

5. Conclusions

NeuroMaps is a novel fingerprint design with the goal to convey a maximum of visual information through a dense custom-made visualization, which is particularly useful in small-multiples or overview visualizations. To this end, we adapt and integrate existing processing techniques in an efficient pipeline. As the selection of techniques represent opportunistic choices, our next steps will include to scrutinize the effectiveness of each stage and subject the approach to a thorough evaluation.

Acknowledgments

This work is partially supported by the HEREDITARY Project, as part of the European Union's Horizon Europe research and innovation programme under grant agreement No GA 101137074. We also thank Mattia Veronese from the University of Padova and his group for their insightful discussions and valuable feedback.

References

[AKM*18] ARSLAN S., KTENA S. I., MAKROPOULOS A., ROBINSON E. C., RUECKERT D., PARISOT S.: Human brain mapping: A systematic comparison of parcellation methods for the human cerebral cortex. *NeuroImage 170* (Apr. 2018), 5–30. doi:10.1016/j.neuroimage.2017.04.014. 3

[AWW*23] AHMAD S., WU Y., WU Z., THUNG K.-H., LIU S., LIN W., LI G., WANG L., YAP P.-T.: Multifaceted atlases of the human brain in its infancy. *Nature Methods 20*, 1 (Jan. 2023), 55–64. doi:10.1038/s41592-022-01703-z. 2

[BTH*24] BOLAÑOS-PUCHET S., TESKA A., HERNANDO J. B., LU H., ROMANI A., SCHÜRMANN F., REIMANN M. W.: Enhancement of brain atlases with laminar coordinate systems: Flatmaps and barrel column annotations. *Imaging Neuroscience 2* (June 2024), imag–2–00209. doi:10.1162/imag_a_00209. 2

[CFR*26] CHAMMA A., FRAU-PASCUAL A., ROTHBERG A., ABADIE A., ABRAHAM A., ET AL.: Nilearn. Zenodo, Jan. 2026. doi:10.5281/zenodo.18159806. 2

[Cra18] CRAMERI F.: Geodynamic diagnostics, scientific visualisation and StagLab 3.0. *Geoscientific Model Development 11*, 6 (June 2018), 2541–2562. doi:10.5194/gmd-11-2541-2018. 3

[CS92] CHANDLER P., SWELLER J.: The Split-Attention Effect as a Factor in the Design of Instruction. *British Journal of Educational Psychology 62*, 2 (1992), 233–246. doi:10.1111/j.2044-8279.1992.tb01017.x. 2

[CS25] CHOU M. S.-Y., SCHULZ H.-J.: Visual Fingerprints for Detecting Data Characteristics. In *2025 IEEE Visualization and Visual Analytics (VIS)* (Nov. 2025), pp. 106–110. doi:10.1109/VIS60296.2025.00027. 2

[DLTVDOCG25] DUPRÉ LA TOUR T., VISCONTI DI OLEGGIO CASTELLO M., GALLANT J. L.: The Voxelwise Encoding Model framework: A tutorial introduction to fitting encoding models to fMRI data. *Imaging Neuroscience 3* (May 2025), imag_a_00575. doi:10.1162/imag_a_00575. 2

[DSF*06] DESIKAN R. S., SÉGONNE F., FISCHL B., QUINN B. T., DICKERSON B. C., ET AL.: An automated labeling system for subdividing the human cerebral cortex on MRI scans into gyral based regions of interest. *Neuroimage 31*, 3 (2006), 968–980. doi:10.1016/j.neuroimage.2006.01.021. 3

[DVEA*96] DRURY H. A., VAN ESSEN D. C., ANDERSON C. H., LEE C. W., COOGAN T. A., LEWIS J. W.: Computerized Mappings of the Cerebral Cortex: A Multiresolution Flattening Method and a Surface-Based Coordinate System. *Journal of Cognitive Neuroscience 8*, 1 (Jan. 1996), 1–28. doi:10.1162/jocn.1996.8.1.1. 2

[FCB*05] FRAZIER J. A., CHIU S., BREEZE J. L., MAKRIS N., LANGE N., ET AL.: Structural Brain Magnetic Resonance Imaging of Limbic and Thalamic Volumes in Pediatric Bipolar Disorder. *American Journal of Psychiatry 162*, 7 (July 2005), 1256–1265. doi:10.1176/appi.ajp.162.7.1256. 3

[FEB*11] FONOV V., EVANS A. C., BOTTERON K., ALMLI C. R., MCKINSTRY R. C., COLLINS D. L.: Unbiased average age-appropriate atlases for pediatric studies. *NeuroImage 54*, 1 (Jan. 2011), 313–327. doi:10.1016/j.neuroimage.2010.07.033. 2

[FHW*94] FRISTON K. J., HOLMES A. P., WORSLEY K. J., POLINE J.-P., FRITH C. D., FRACKOWIAK R. S. J.: Statistical parametric maps in functional imaging: A general linear approach. *Human Brain Mapping 2*, 4 (Jan. 1994), 189–210. doi:10.1002/hbm.460020402. 2

[Fuk13] FUKUNAGA K.: *Introduction to Statistical Pattern Recognition*. Elsevier, 2013. 3

[GLS17] GRAMAZIO C. C., LAIDLAW D. H., SCHLOSS K. B.: Colorgorical: Creating discriminable and preferable color palettes for information visualization. *IEEE TVCG 23*, 1 (Jan. 2017), 521–530. doi:10.1109/TVCG.2016.2598918. 3

[GSM*07] GOLDSTEIN J. M., SEIDMAN L. J., MAKRIS N., AHERN T., O'BRIEN L. M., CAVINESS JR V. S., KENNEDY D. N., FARAONE S. V., TSUANG M. T.: Hypothalamic abnormalities in schizophrenia: Sex effects and genetic vulnerability. *Biological psychiatry 61*, 8 (2007), 935–945. doi:10.1016/j.biopsych.2006.06.027. 3

[GVR*15] GORGOLEWSKI K. J., VAROQUAUX G., RIVERA G., SCHWARZ Y., GHOSH S. S., ET AL.: NeuroVault. org: A web-based repository for collecting and sharing unthresholded statistical maps of the human brain. *Frontiers in neuroinformatics 9* (2015), 8. doi:10.3389/fninf.2015.00008. 2

[HLG*12] HAWRYLYCZ M. J., LEIN E. S., GUILLOZET-BONGAARTS A. L., SHEN E. H., NG L., MILLER J. A., ET AL.: An anatomically comprehensive atlas of the adult human brain transcriptome. *Nature 489*, 7416 (Sept. 2012), 391–399. doi:10.1038/nature11405. 2

[HLM] HABES M., LANCASTER J. L., MARTINEZ M. J.: Mango. https://mangoviewer.com/index.html. 2

[KSLA*21] KOHN N., SZOPINSKA-TOKOV J., LLERA ARENAS A., BECKMANN C., ARIAS-VASQUEZ A., AARTS E.: Multivariate associative patterns between the gut microbiota and large-scale brain network connectivity. *Gut Microbes 13*, 1 (Jan. 2021), 2006586. doi:10.1080/19490976.2021.2006586. 4

[Mad15] MADAN C. R.: Creating 3D visualizations of MRI data: A brief guide. *F1000Research 4* (Aug. 2015), 466. doi:10.12688/f1000research.6838.1. 2

[MBS*21] MAITIN-SHEPARD J., BADEN A., SILVERSMITH W., PERLMAN E., COLLMAN F., ET AL.: Google/neuroglancer:. Zenodo, Oct. 2021. doi:10.5281/zenodo.5573294. 2

[MGK*06] MAKRIS N., GOLDSTEIN J. M., KENNEDY D., HODGE S. M., CAVINESS V. S., FARAONE S. V., TSUANG M. T., SEIDMAN L. J.: Decreased volume of left and total anterior insular lobule in schizophrenia. *Schizophrenia research 83*, 2-3 (2006), 155–171. doi:10.1016/j.schres.2005.11.020. 3

[Rao48] RAO C. R.: The Utilization of Multiple Measurements in Problems of Biological Classification. *Journal of the Royal Statistical Society: Series B (Methodological) 10*, 2 (July 1948), 159–193. doi:10.1111/j.2517-6161.1948.tb00008.x. 3

[Ror25] RORDEN C.: From MRIcro to MRIcron: The evolution of neuroimaging visualization tools. *Neuropsychologia 207* (Jan. 2025), 109067. doi:10.1016/j.neuropsychologia.2025.109067. 2

[Sb85] SUZUKI S., BE K.: Topological structural analysis of digitized binary images by border following. *Computer Vision, Graphics, and Image Processing 30*, 1 (Apr. 1985), 32–46. doi:10.1016/0734-189X(85)90016-7. 3

[SG64] SAVITZKY ABRAHAM., GOLAY M. J. E.: Smoothing and Differentiation of Data by Simplified Least Squares Procedures. *Analytical Chemistry 36*, 8 (July 1964), 1627–1639. doi:10.1021/ac60214a047. 3

[Sil21] SILVERSMITH W.: Cc3d: Connected components on multilabel 3D & 2D images. Zenodo, Sept. 2021. doi:10.5281/zenodo.5719536. 3

[Smi04] SMITH S. M.: Overview of fMRI analysis. *British Journal of Radiology 77*, suppl_2 (Dec. 2004), S167–S175. doi:10.1259/bjr/33553595. 2

[SV89] SNYDER J. P., VOXLAND P. M.: An album of map projections. *Professional Paper*, 1453 (1989). doi:10.3133/pp1453. 2

[SYB*24] SCHLEGEL P., YIN Y., BATES A. S., DORKENWALD S., EICHLER K., ET AL.: Whole-brain annotation and multi-connectome cell typing of Drosophila. *Nature 634*, 8032 (Oct. 2024), 139–152. doi:10.1038/s41586-024-07686-5. 2

[WQZ*25] WANG A. Z., QUADRI G. J., ZHU M., TSENG C., SZAFIR D. A.: Characterizing Visualization Perception with Psychological Phenomena: Uncovering the Role of Subitizing in Data Visualization. *IEEE Transactions on Visualization and Computer Graphics* (2025), 1–11. doi:10.1109/TVCG.2025.3634807. 4